On the use of 3-D electrodes and pulsed voltage for the process intensification of alkaline water electrolysis

Q. de Radiguès, G. Thunis and J. Proost*

Université catholique de Louvain (UCLouvain), Division of Materials and Process Engineering, Place Sainte Barbe, 2, 1348 Louvain-la-Neuve, Belgium

Abstract

In this work, the potential of process intensification of alkaline water electrolysis has been studied when using 3-D nickel electrodes. First of all, it was shown that such macro-porous, 3-D electrodes, when used in combination with forced electrolyte flow, can have a strong impact on the hydrogen generation performance of the process. For optimal conditions of the imposed Reynolds numbers of both the catholyte and anolyte flow, a 45 % increase in current was measured as compared to state-of-the-art 2-D electrodes for a cell potential of 2 V, the latter being a typical value for industrial electrolysers. For the 2-D electrodes, forced flow did not induce any significant improvement. Secondly, the use of pulsed electrical power has been studied as well, with pulse widths in the range 2 - 200 ms. A significant synergistic effect was observed when using 3-D electrodes in combination with both forced flow and pulsed voltage, allowing in the case of 2 ms pulses an almost fivefold increase in current at 2 V.

Keywords: renewable hydrogen, alkaline water electrolysis, pulsed voltage, 3-D electrodes, process intensification

* Corresponding author: joris.proost@uclouvain.be

1. Introduction

In order for hydrogen to serve as an energy vector in the transition to renewable energies, the water electrolysis process has to be intensified: it has to become more performing in terms of energy use, and installation has to become more compact. Water electrolysis has already been extensively reviewed in the literature [1–6]. This work focusses in particular on alkaline water electrolysis (AEL), being the state-of-the-art technology for producing hydrogen at an industrial scale. It has lower specific investments costs than its two competing technologies: Proton Exchange Membrane (PEM) electrolyzers and Solid Oxide Electrolyzers [1]. AEL is based on high durability nickel electrodes without the need for expensive noble metals as electrocatalysts [4]. In order to increase the electrocatalytic activity of nickel, its surface area can be enhanced, for instance by using Raney nickel [7], by leaching Al previously deposited on Ni by PVD [8] or by leaching zeolites selectively from an electrodeposited nickel/zeolite electrode [9]. Creating nano-sized metallic Ni catalysts can dramatically improve the current increase at higher overpotential owing to larger surface areas [2]. To increase even further the active surface area, flow-through electrodes can be used where the entire cell compartment is filled with an active electrode through which the electrolyte flows. Different types of electrodes can be used such as copper screens, metallized particles, porous carbon and nickel foams [10–15]. Both on copper screens [10] and porous carbon [12–14], the highest electrocatalytic activity was achieved for the highest surface area. The reticulated vitreous carbon (RVC) was coated with black nickel [7] and Watts nickel [8] to increase the rate of hydrogen production. The electrode morphology is seen to affect the ohmic resistance of the water electrolysis cell, with the nickel foam exhibiting the lowest initial ohmic resistance, 2% lower than the expanded mesh[9].

Gas bubble formation on the electrode surface and its insufficient evacuation are major causes of extra ohmic losses [16] : bubbles will disturb the current distribution in the cell, and isolate active sites from reactive ions [6]. The produced gas bubbles can be swept from the electrode surface either by circulating the solution or enhancing the convection with a magnetic field [17]. The ohmic resistance of the electrolysis cell is governed by the void fraction of the electrolyte between the electrodes. When forcing the electrolyte flow, the associated reduction in ohmic resistance is attributed to the reduced time each bubble spends in the inter-electrode gap [15]. Circulating the solution will also eliminate concentration differences in the fluid [18]. Experimentally, it has been found that gas bubbles accumulate in RVC electrodes under

stationary conditions. Starting the electrolyte flow leads to a sharp decrease in cell potential, showing the positive impact of electrolyte flow [14]. Some authors have also attributed the discrepancy between theoretical simulation and experiments to trapped gas bubbles within the pores of the electrode [12,13].

A third way to increase the hydrogen generation performance of water electrolysis is by using pulsed electrical power. Pulsed power can be beneficial in three independent ways: by avoiding the formation of an electrical double layer and the associated capacitive losses [3], by reducing the concentration overpotential [19], and by helping the bubbles to detach from the electrode and hence restore the electrochemically active area [20,21]. Vanags *et al.* claim that when using short pulses, the charging of the cell can be separated from the electrochemical reactions in water electrolysis process [22]. Pulsed electrolysis has been studied for quite some time in water electrolysis [23] but also for metal plating [24,25]. The effect of current ripples has also been assessed in PEM fuel cells [26]. In this last application, mass transport is significant only at frequencies below 100 mHz, while charge transport becomes dominant at frequencies above 1 Hz. This is consistent with results in the electroplating application: the electrical double layer charges in a few µs while a few seconds is needed to build up the mass transfer layer [25].

The reported effects of applying pulsed voltage vary widely. Shaaban has found pulsed DC to be detrimental for frequencies from 10 Hz to 40 kHz [23]. However, this author applied 0 V cell voltage between two pulses. This can revert the electrode polarity, creating oxygen at the cathode [22]. Dobó *et al.* have shown that in the case of sinusoidal waves, lower frequencies enhance the gas production yield [27] but the benefits are limited. For this reason, square pulses are generally preferred since they allow for an improved energy transfer [3]. Naohiro *et al.* used pulses of 300 ns allowing to increase the efficiency of the electrolysis process to 45 %, as compared to 40 % for DC electrolysis [28]. Using pulse width modulation to obtain a frequency of 60 kHz, Mandal *et al.* were able to increase the gas production rate by 34 % compared to DC power [29]. Finally, Dharmaraj *et al* claim to be able to reduce the power consumption from 18 W to 0.57 W using 200 ns pulses at 100 MHz, while keeping the produced gas rate constant [30]. Using a MOSFET driver circuit, Demir *et al.* applied square pulses up to 1200 kHz achieving a 20-25 % lower energy consumption for 50 % duty cycles, compared to DC current [21].

After presenting the experimental set-up and procedures, this work will be divided in two main parts. In the first part, we will show the advantage of 3-D nickel electrodes compared to state-of-the-art 2-D electrodes. We will also show that, using 3-D electrodes, forced electrolyte flow can have a significant impact on the water electrolysis performance. In the second part, we will show how the use of pulsed electrical power can further increase the efficiency of H_2 generation when combined with both 3-D electrodes and forced flow.

2. Experimental details

Pictures of the experimental setup are shown in Fig. 1. It is comparable to the setup we already described in earlier work [31]. It consists of a commercial filter press cell (Micro Flow cell from Electrocell) shown schematically at the bottom left of Fig. 1. A Fumasep FAA-3-PK-130 membrane separated the two compartments of the cell. Unless specified otherwise, the tested 3-D electrodes have been inserted in both the cathodic and anodic compartment of the cell. The electrodes were placed at the center of their respective cathodic and anodic compartment and compressed to a nickel current collector plate. Fig. 2 shows SEM micrographs of the different 3-D electrodes that have been tested. They are made of pure nickel and commercialized by Alantum. The geometrical properties of the 3-D electrodes are described in Table 1. Two different 2-D electrodes were used: the “2-D mesh” was a reference was a state-of-the-art wire mesh of 0.2 dm^2 surface area and the “2-D gap” was the bare current collector plate. The electrical contact made by these collectors generated a current flow perpendicular to the electrolyte flow (flow-by configuration). An upstream flow was imposed to avoid gas accumulation in the cell compartments. The electrochemical cell was inserted into a hydraulic circuit, shown in Fig. 1 at the top. It includes two pumps forcing the circulation of the electrolyte independently in each compartment of the filter press cell. The electrolyte then flows back into a 1 L stirred tank. The pumping rate was adjusted in order to obtain an electrolyte flow varying from 6 to 14 mL/s in both the catholyte and anolyte compartments. Some experiments were also performed without forced flow, relying on natural convection. The tanks were airtight, and nitrogen was blown in the catholyte prior to each experiment in order to avoid the parasitic reduction of dissolved oxygen to water.

The electrolyte used was a 1.0 M KOH solution (>85 %, Carl Roth). The experiments were performed using a Solartron-XM potentiostat. In the Cyclo-Voltammetry (CV) experiments,

the cell voltage was varied from 1.23 V (which is the equilibrium cell voltage for water electrolysis) to 3.0 V at 0.1 V/s in steps of 2.44 mV. The same potentiostat was also used to apply a pulsed voltage to the cell, as shown in Fig. 6 (left). During such pulsed experiments, the cell voltage was varied from 1.2 V to 3.0 V in steps of 100 mV. In the interval time (t_{off}) between each voltage step, a base voltage 1.2 V was reimposed. The pulse time (t_{on}) was always the same as the interval time. Three different pulse widths have been studied (2, 20 and 200 ms), and the pulses were applied such that the polarity of the electrodes remained the same.

3. Results and discussion

3.1. 3-D electrodes and forced flow

Fig. 3 shows a typical result of a CV experiment during forced flow, representing the measured current *I*, which can be taken as indicative for the hydrogen production rate, vs. the applied cell potential *U*. Three types of experiments have been superimposed : 2-D electrodes on both the cathodic and anodic side, 1200 µm and 580 µm pore sized 3-D electrodes on the cathodic side and a 2-D electrode on the anode side, and 1200 µm and 580 µm pore sized 3-D electrodes on the both the cathodic anodic side. Comparing the 2-D and 3-D electrodes, we can clearly see that for the same applied cell voltage, the produced current increases significantly with the use of 3-D electrodes during forced flow. Indeed, from the Butler-Volmer equation, the current density *j* of an electrochemical reaction increases exponentially with its required overpotential :

$$j = j_0 \left\{ \exp\left[\frac{(1-\alpha_a)zF}{RT\eta_a}\right] - \exp\left[-\frac{\alpha_c zF}{RT\eta_c}\right] \right\} \quad (1)$$

with j_0 the exchange current density, η_a and η_c the anodic and cathodic overpotential, α_a and α_c the anodic and cathodic symmetry factor, z the number of exchanged electrons, F and R the Faraday and universal gas constant respectively, and T the absolute temperature. By increasing the surface area using 3-D electrodes, we decrease the current density for the same measured current. This will therefore decrease the required overpotential, decreasing in turn the overall electrical consumption of the cell. It also explains the higher measured current for the same applied cell voltage when using 3-D electrodes compared with state-of-the-art 2-D electrodes.

The effect of forced electrolyte flow is further illustrated in Fig. 4. It shows typical CV curves for 2-D electrodes (left-hand side) and 450 µm pore sized 3-D electrodes (right-hand side), both under Natural Convection (NC) and for two different flow rates. The pore size chosen for the 3-D electrodes was 450 µm, as this yielded the highest surface area (see Table 1). The flow rates are indicated using the dimensionless Reynolds number *Re*, based on the hydraulic diameter D_h of the cell:

$$Re = \frac{\rho v D_h}{\mu} \quad (2)$$

$$v = \frac{Q}{l\,h} \quad (3)$$

$$D_h = \frac{4\,l\,h}{l+h} \quad (4)$$

with ρ the density of the electrolyte, Q the volumetric flow rate, l and h the width and height of the electrode compartment, and μ the electrolyte dynamic viscosity. For our 1.0 M KOH solution, values for ρ and μ were taken as 1.04 10^3 (kg/m³) and 1 10^{-3} kg/(m*s), respectively [32]. Similarly as in Fig. 3, Fig. 4 shows for the same cell voltage a significant increase in current when 3-D electrodes are used instead of state-of-the-art 2-D electrodes. For instance, at 2.0 V, which is a typical cell voltage during industrial alkaline water electrolysis, the current at the highest flow rate amounts to 344 mA for the 3-D electrodes. This is 45 % higher than the current value of 237 mA obtained for the 2-D electrodes under similar flow conditions.

At the same time, Fig. 4 also clearly indicates that in the case of 3-D electrodes, the use of a forced electrolyte flow is absolutely mandatory. If not, its performance becomes even worse than for classical 2-D electrodes. In this respect, Fig. 5 compares the variation of the current *I* measured at 2.0 V with both the catholyte and anolyte flow rate for 2-D (left) and 450 µm pore size 3-D (right) electrodes. Note that *Re* = 0 corresponds to Natural Convection (NC), i.e. when no forced flow is applied. This explicitly confirms what was already anticipated from Fig. 4: the performance of 3-D electrodes decreases dramatically under natural convection. On the other hand, the influence of forced flow is barely visible for the 2-D electrodes. Looking more into detail at the influence of forced flow for 3-D electrodes, we can see that a moderate cathodic flow is already sufficient to drastically increase the H_2 generation performance, whereas an important anodic flow is necessary. Finally, the mean current measured at 2 V in the plateau

region is 227 ± 8 mA for the 2-D and 330 ± 30 mA for the 3-D electrodes. This quantitatively confirms the 45 % improvement for the latter already observed in Fig. 4 with respect to state-of-the-art 2-D electrodes.

Based on Fig. 4 and Fig. 5, we can therefore reliably conclude that the electrolyte flow rate significantly influences the cell performance when using 3-D electrodes, but not so much in the case of state-of-the-art 2-D electrodes. We attribute this to the fact that, in the case of 3-D electrodes, the produced gas bubbles are more easily trapped inside the 3-D structure, while the use of a 2-D wire mesh allows them to escape out of the cell more easily. This explains also why forced flow is not a state-of-the-art practice in industry: it only makes sense when using high surface area, macro-porous 3-D electrodes, where produced gas bubbles have to be forced out of the 3-D structure. If not, such trapped gas bubbles risk indeed to "insulate" useful electrode surface area, thereby decreasing the electrochemically active surface area and increasing the overpotential. By forcing the gas bubbles out of the 3-D structure, the entire electrode surface area becomes available again for the electron transfer, using the full potential of 3-D electrodes. In other words, the two technologies (3-D electrodes and forced flow) always need to be used in combination.

3.2. Pulsed voltage

In order to increase even more the H_2 generation performance of the cell, we have also studied the effect of applying a pulsed DC voltage. A typical result is shown in Fig. 6 for 3 different pulse widths. It can be seen that a negative current is always being measured during t_{off}. This can be due to a transient electrical effect or, in the worst case, the inverse reaction taking place, i.e. the consumption of hydrogen and oxygen to produce water. To take into account this worst-case scenario, we have computed the mean positive current during t_{on}, the mean negative current during t_{off} and, as illustrated in Fig. 7, taken the sum of both at an applied cell voltage of 2.0 V as a characteristic figure of merit for the resulting current.

Fig. 8 then shows the final results for both the 2-D and 3-D electrodes with different pore sizes. In the case of the 200 ms and 20 ms pulses, a decrease of the average current is observed in all cases. This is due to the increase of the current during t_{off} being more important than the increase of current during t_{on}. For the 2 ms pulses however, an increase of the average current is observed, even when taking into account the current during t_{off}. In this case, we can also see

that for the 2-D electrodes, the current is the same as the one obtained without pulsation (CV), whereas a significant increase is observed for the 3-D electrodes. For the latter, the improvement is more important when decreasing the pore sizes. Moreover, for the 3-D electrodes with the smallest pore size (580 µm and 450 µm), the increase in current becomes especially pronounced at higher flow rates, whereas the impact of the flow rate is barely visible on the current obtained without pulsation for bigger pore sizes and 2-D electrodes.

At this stage, it is still difficult to quantitatively compare these results to reported effects of pulsed power on water electrolysis from the literature. Qualitatively, our own findings do confirm the general tendancy that the hydrogen generation efficiency improves when using square pulses of high frequency that preserve the electrode polarity. The specific novelty of our work is that we have convincingly demonstrated that there is a combined, synergistic effect of all 3 technologies: 3-D electrodes, forced flow and pulsed voltage. In this respect, Fig. 8 indicates an almost fivefold increase in current with respect to 2-D electrodes when using 450 µm pore size 3-D electrodes, high forced flow and 2 ms electrical pulses.

4. Conclusions

This paper has studied the possibility of process intensification of alkaline water electrolysis using 3-D electrodes, forced flow and pulsed voltage. In the first part, we have looked at conventional DC voltage (without pulses). In this case, the use of 3-D electrodes was observed to have a strong positive impact on the electrical cell performance. This was attributed to the increase in active surface area, which decreases the current density for the same amount of current. This in turn decreases the overpotential of the reaction, according to the Butler-Volmer equation. Moreover, in the case of 3-D electrodes, forced electrolyte flow was shown to have a significant impact on the cell performance, while almost no flow effect was observed for 2-D electrodes. This was attributed to the usefulness of forced electrolyte flow for evacuating the produced gas bubbles out of the structure of the 3-D electrode. In the second part, we have studied the impact of pulsed voltage on alkaline water electrolysis. We have seen that in all cases, lower frequencies (200 ms and 20 ms pulse time) decrease the electrical performance of the process, while a 2 ms pulse time has a positive effect. We also observed a strong synergistic effect when combining 3-D electrodes with forced flow and pulsed voltage, highlighting the very promising potential for process intensification of all three technologies when used together.

Acknowlegdements

The authors acknowledge financial support of the Public Service of Wallonia – Department of Energy and Sustainable Building through the project WallonHY.

References

[1] Buttler A, Spliethoff H. Current status of water electrolysis for energy storage, grid balancing and sector coupling via power-to-gas and power-to-liquids: A review. Renew Sustain Energy Rev 2018;82:2440–54. doi:10.1016/J.RSER.2017.09.003.

[2] Gong M, Wang DY, Chen CC, Hwang BJ, Dai H. A mini review on nickel-based electrocatalysts for alkaline hydrogen evolution reaction. Nano Res 2016;9:28–46. doi:10.1007/s12274-015-0965-x.

[3] Monk N, Watson S. Review of pulsed power for efficient hydrogen production. Int J Hydrogen Energy 2016;41:7782–91. doi:10.1016/j.ijhydene.2015.12.086.

[4] Vincent I, Bessarabov D. Low cost hydrogen production by anion exchange membrane electrolysis: A review. Renew Sustain Energy Rev 2018;81:1690–704. doi:10.1016/j.rser.2017.05.258.

[5] Carmo M, Fritz DL, Mergel J, Stolten D. A comprehensive review on PEM water electrolysis. Int J Hydrogen Energy 2013;38:4901–34. doi:10.1016/j.ijhydene.2013.01.151.

[6] Wang M, Wang Z, Gong X, Guo Z. The intensification technologies to water electrolysis for hydrogen production - A review. Renew Sustain Energy Rev 2014;29:573–88. doi:10.1016/j.rser.2013.08.090.

[7] Rami A, Lasia A. Kinetics of hydrogen evolution on Ni-Al alloy electrodes. J Appl Electrochem 1992;22:376–82. doi:10.1007/BF01092692.

[8] Kjartansdóttir CK. Development of Hydrogen Electrodes for Alkaline Water Electrolysis 2014:189.

[9] Xie Z, He P, Du L, Dong F, Dai K, Zhang T. Comparison of four nickel-based electrodes for hydrogen evolution reaction. Electrochim Acta 2013;88:390–4. doi:10.1016/j.electacta.2012.10.057.

[10] El-Deab MS, El-Shakre ME, El-Anadouli BE, Ateya BG. Hydrogen evolution on stacked copper screen electrodes from flowing alkaline solutions. Int J Hydrogen Energy 1996;21:273–80. doi:10.1016/0360-3199(95)00084-4.

[11] El-Anadouli BE, Khader MM, Saleh MM, Ateya BG. Hydrogen evolution on metallized plastic packed bed electrodes. Electrochim Acta 1991;36:1899–905. doi:10.1016/0013-4686(91)85070-N.

[12] El-Deab MS, Saleh MM. Electrocatalytic production of hydrogen on reticulated vitreous carbon. Int J Hydrogen Energy 2003;28:1199–206. doi:10.1016/S0360-3199(03)00002-

8.

[13] El-Deab MS, El-Shakre ME, El-Anadouli BE, Ateya BG. Electrolytic generation of hydrogen on Pt-loaded porous graphite electrodes from flowing alkaline solutions. J Appl Electrochem 1996;26:1135–7. doi:10.1007/BF00243738.

[14] Saleh MM, El-Ankily MH, El-Deab MS, El-Anadouli BE. Electrocatalytic activity of metal-loaded reticulated vitreous carbon electrodes for hydrogen evolution from flowing alkaline solutions. Bull Chem Soc Jpn 2006;79:1711–8. doi:10.1246/bcsj.79.1711.

[15] Phillips R, Edwards A, Rome B, Jones DR, Dunnill CW. Minimising the ohmic resistance of an alkaline electrolysis cell through effective cell design. Int J Hydrogen Energy 2017;42:23986–94. doi:10.1016/j.ijhydene.2017.07.184.

[16] Mazloomi SKK, Sulaiman N. Influencing factors of water electrolysis electrical efficiency. Renew Sustain Energy Rev 2012;16:4257–63. doi:10.1016/j.rser.2012.03.052.

[17] Matsushima H, Iida T, Fukunaka Y. Observation of bubble layer formed on hydrogen and oxygen gas-evolving electrode in a magnetic field. J Solid State Electrochem 2012;16:617–23. doi:10.1007/s10008-011-1392-x.

[18] Zeng K, Zhang D. Recent progress in alkaline water electrolysis for hydrogen production and applications. Prog Energy Combust Sci 2009;36:307–26. doi:10.1016/j.pecs.2009.11.002.

[19] Vincent I, Choi B, Nakoji M, Ishizuka M, Tsutsumi K, Tsutsumi A. Pulsed current water splitting electrochemical cycle for hydrogen production. Int J Hydrogen Energy 2018;43:10240–8. doi:10.1016/j.ijhydene.2018.04.087.

[20] Vilasmongkolchai T, Songprakorp R, Sudaprasert K. The Behaviour of Gas Bubble during Rest Period of Pulse-Activated Electrolysis Hydrogen Production. MATEC Web Conf 2016;77:1–5. doi:10.1051/matecconf/20167714001.

[21] Demir N, Kaya MF, Albawabiji MS. Effect of pulse potential on alkaline water electrolysis performance. Int J Hydrogen Energy 2018;43:17013–20. doi:10.1016/j.ijhydene.2018.07.105.

[22] Vanags M, Kleperis J, Bajars G. Water Electrolysis with Inductive Voltage Pulses. Electrolysis, 2012, p. 19–44. doi:http://dx.doi.org/10.5772/57353.

[23] Shaaban AH. Water Electrolysis and Pulsed Direct Current. J Electrochem Soc 1993;140:2863–7. doi:10.1149/1.2220923.

[24] Puippe JC, Ibl N. Influence of charge and discharge of electric double layer in pulse plating. J Appl Electrochem 1980;10:775–84. doi:10.1007/BF00611281.

[25] Ibl N. Some Theoretical a Aspects of Pulse Electrolysis. Surf Technol 1980;10:81–104.

[26] Ferrero R, Marracci M, Prioli M, Tellini B. Simplified model for evaluating ripple effects on commercial PEM fuel cell. Int J Hydrogen Energy 2012;37:13462–9. doi:10.1016/j.ijhydene.2012.06.036.

[27] Dobó Z, Palotás ÁB. Impact of the voltage fluctuation of the power supply on the efficiency of alkaline water electrolysis. Int J Hydrogen Energy 2016;41:11849–56. doi:10.1016/j.ijhydene.2016.05.141.

[28] Shimizu N, Hotta S, Sekiya T, Oda O. A novel method of hydrogen generation by water electrolysis using an ultra-short-pulse power supply. J Appl Electrochem 2006;36:419–23. doi:10.1007/s10800-005-9090-y.

[29] Mandal B, Sirkar A, Shau A, Ray P. Effects of Geometry of Electrodes and Pulsating DC Input on Water Splitting for Production of Hydrogen. Int J Renew Energy Res 2012;2:1–4.

[30] Dharmaraj CH, Adishkumar S. Economical hydrogen production by electrolysis using nano pulsed DC. Int J Energy Environ 2012;3:129–36.

[31] de Radiguès Q, Santoro R, Proost J. Kinetic transitions during Ag and Cu electrorecovery on reticulated vitreous carbon electrodes in flow-by mode. Chem Eng J 2010;162. doi:10.1016/j.cej.2010.05.046.

[32] Occidental Chemical Corporation (OxyChem). Caustic Potash Handbook. 2018.

Table 1 : Geometrical properties of the 3-D Ni electrodes

Pore size (µm)	**Thickness (mm)**	**Specific surface area (m^{-1})**	**Developed surface area (dm^2)**
2500	4.5	1480	0.8
1200	6	4300	3.1
800	5	6000	3.7
450	4.8	7800	4.6
580	5.7	6900	4.8

Table 2: Parameters of Pulse time (t_{on}) and Interval time (t_{off}) for the various frequencies

	200 ms	**20 ms**	**2 ms**
Pulse time (t_{on})	0.2 s	$2\ 10^{-2}$ s	$2\ 10^{-3}$ s
Interval time (t_{off})	0.2 s	$2\ 10^{-2}$ s	$2\ 10^{-3}$ s

Figure legends

Fig. 1. Lab-scale experimental set-up used for alkaline water electrolysis.

Fig. 2. SEM micrographs of the 3-D Ni electrodes with different pore sizes.

Fig. 3. Result of a typical CV experiment: measured current vs. applied cell potential for "2-D gap" electrodes, 3-D electrodes on the cathode side, and 3-D electrodes on both cathode and anode side (Re 800).

Fig. 4. Measured current I vs. applied cell potential U for "2-D mesh" electrodes (left-hand side) and 450 µm pore sized 3-D electrodes (right-hand side), both under Natural convection (NC) and for two different forced flow rates.

Fig. 5. Influence of both anolyte (Re_A) and catholyte (Re_C) flow rate on the measured current I at 2 V for "2-D mesh" electrodes (left-hand side) and 450µm pore sized 3-D electrodes (right-hand side). $Re = 0$ corresponds to Natural Convection (NC), i.e. when no forced flow is applied.

Fig. 6. Form of pulsed electrical signals for the different pulse widths (2 ms on top, 20 ms in the middle and 200 ms at the bottom), with the applied voltage (V) on the left hand side and the current response (A) on the right hand side.

Fig. 7. Calculation method used to obtain a characteristic average current value at 2V during pulsed experiments, explicitly taking into account the negative current observed during t_{off}.

Fig. 8. Influence of using a pulsed electrical signal on the measured current at 2V, using the same cathodic and anodic flow rate for "2-D gap" electrodes and 2500 µm, 580 µm and 450 µm pore sized 3-D electrodes. CV = conventional Cyclo-Voltammetry, i.e. no pulse; NC = Natural Convection, i.e. no electrolyte flow.

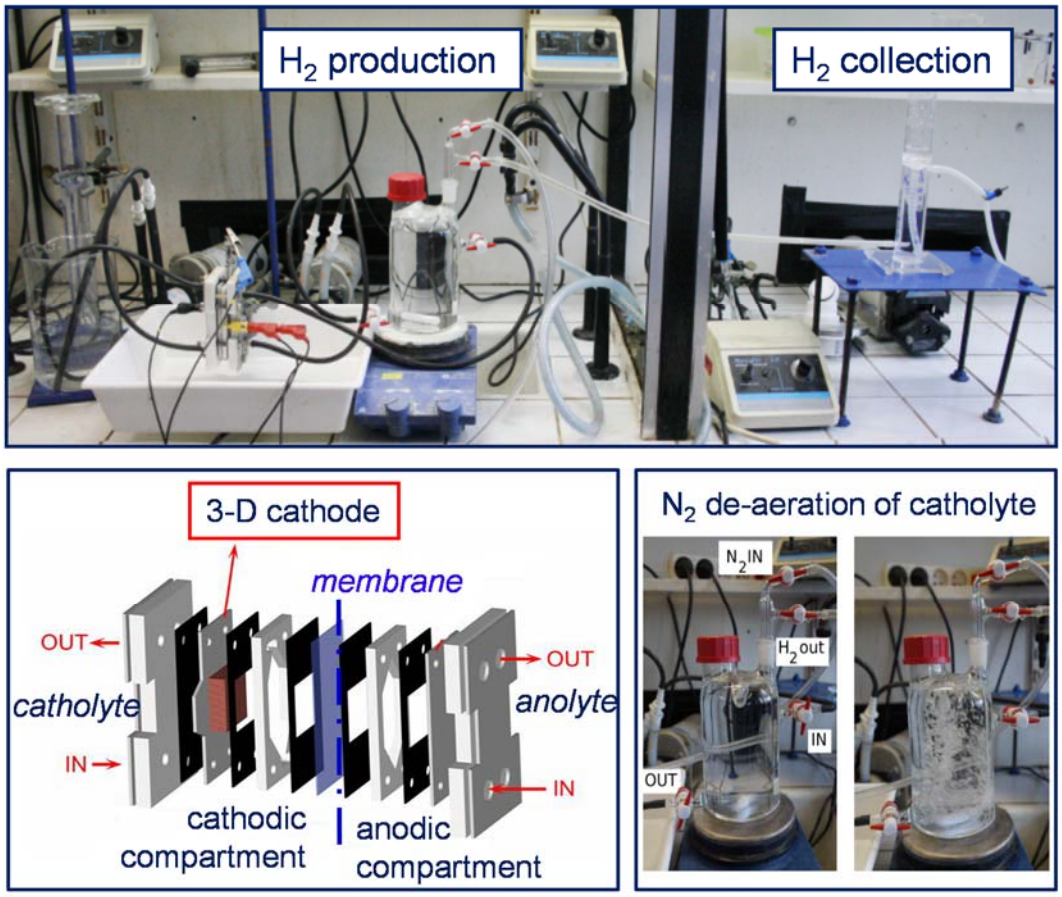
H_2 production
H_2 collection
3-D cathode
membrane
OUT
catholyte
IN
OUT
anolyte
IN
cathodic compartment
anodic compartment
N_2 de-aeration of catholyte
N_2 IN
H_2 out
IN
OUT

Figure 1

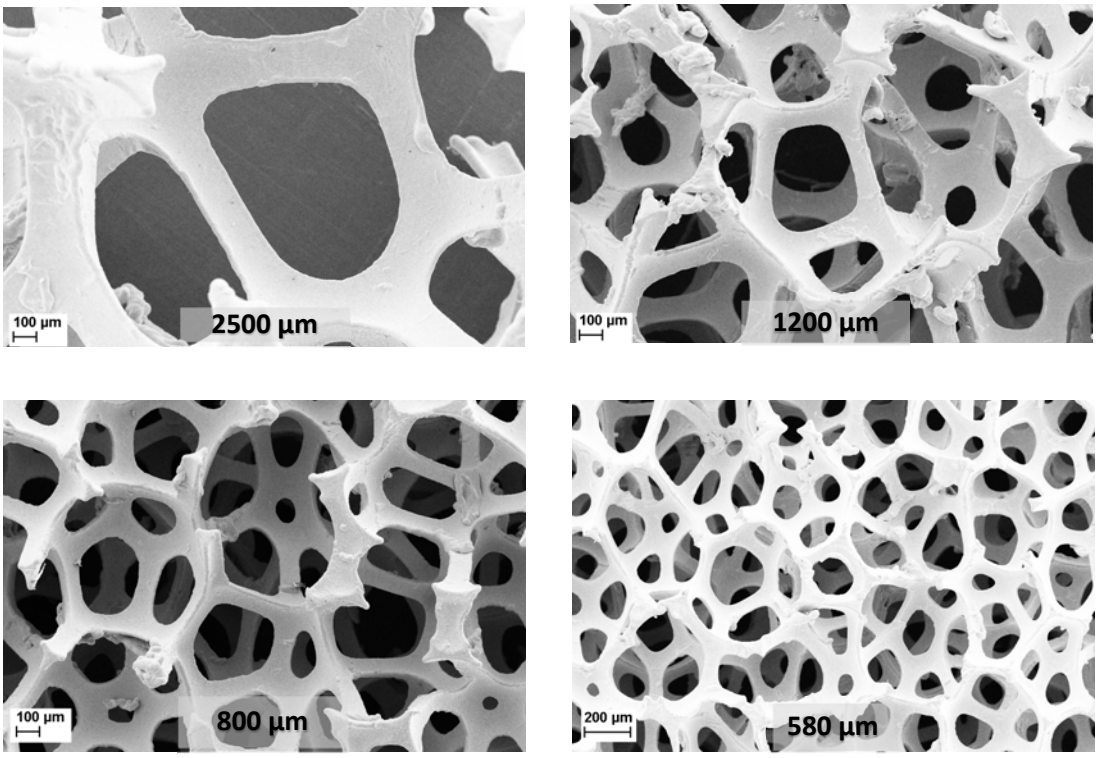

Figure 2

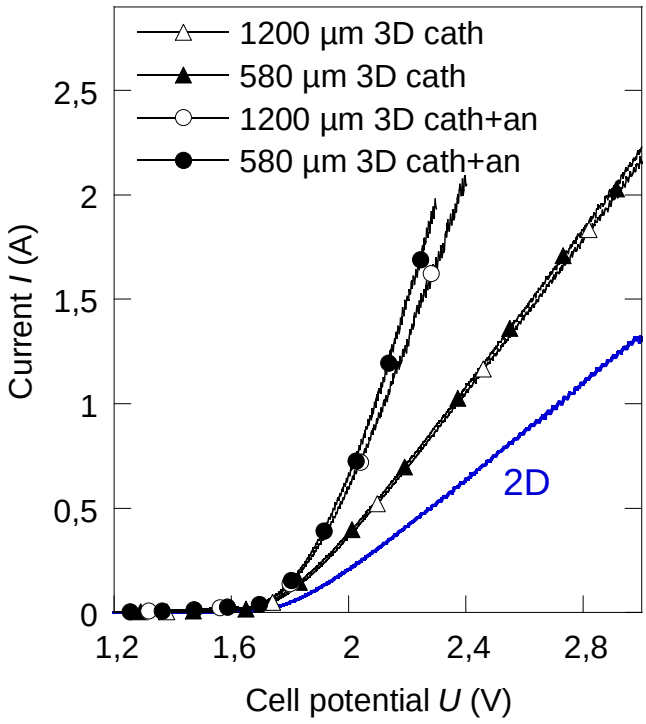
1200 µm 3D cath
580 µm 3D cath
1200 µm 3D cath+an
580 µm 3D cath+an
2D
Current I (A)
Cell potential U (V)
0
0,5
1
1,5
2
2,5
1,2
1,6
2
2,4
2,8

Figure 3

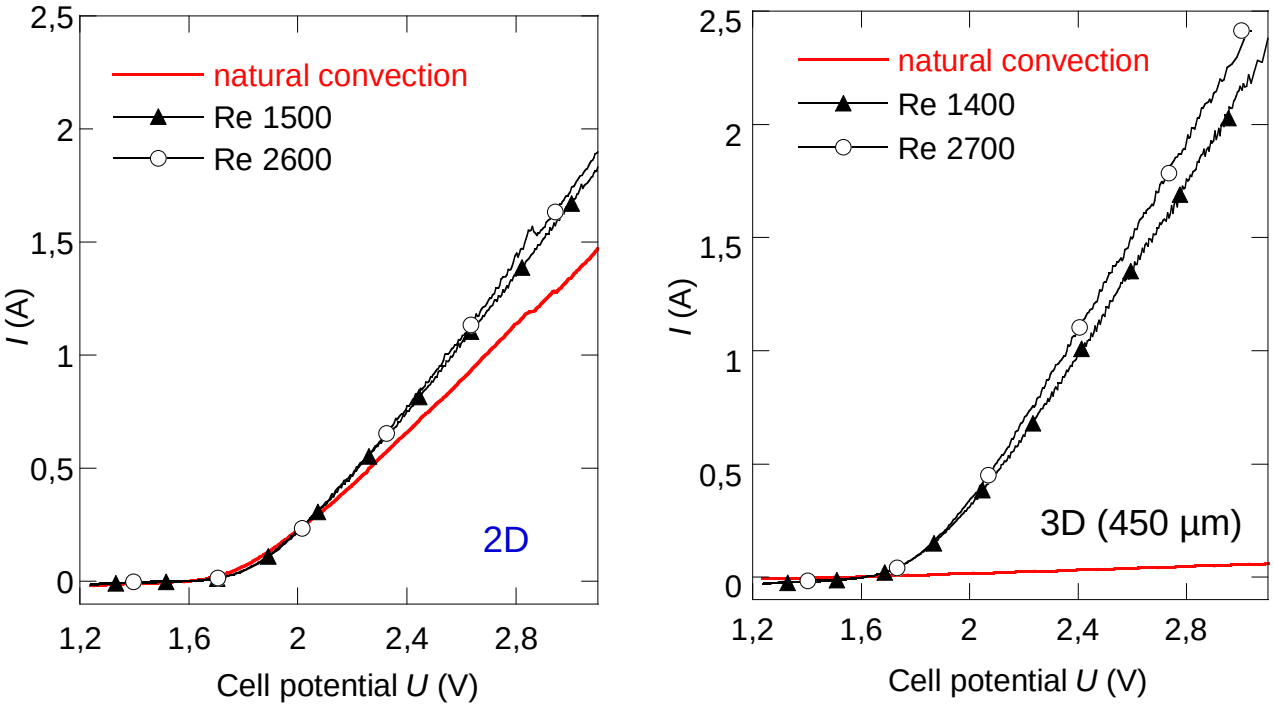
natural convection
Re 1500
Re 2600
2D
I (A)
Cell potential U (V)
natural convection
Re 1400
Re 2700
3D (450 µm)
I (A)
Cell potential U (V)

Figure 4

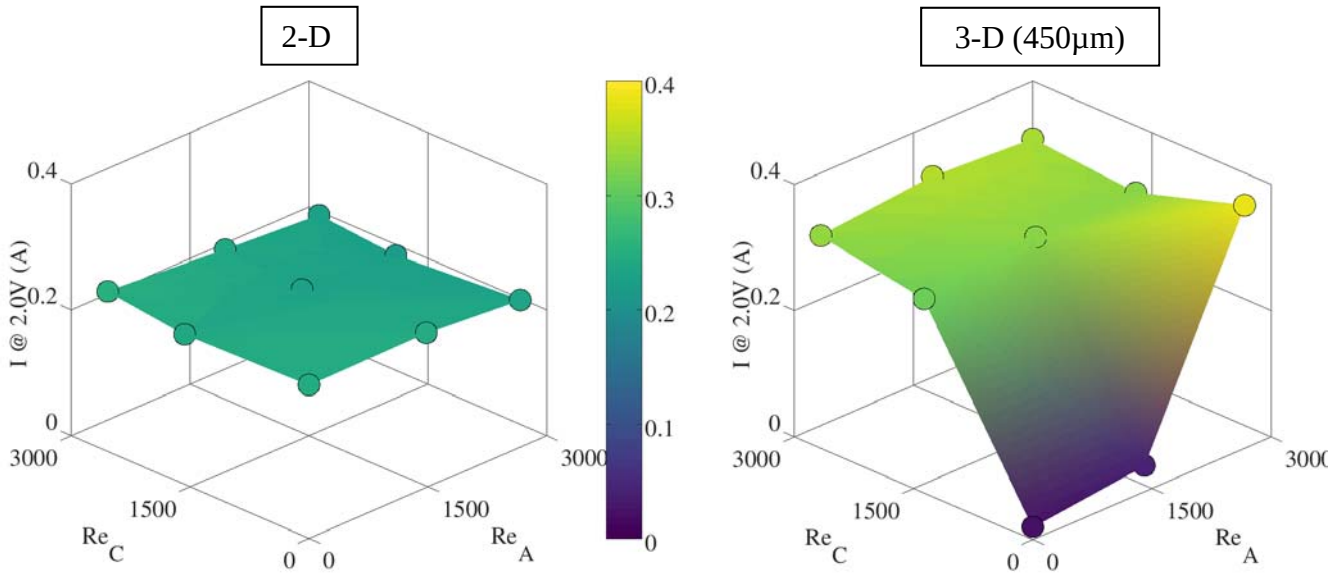

Figure 5

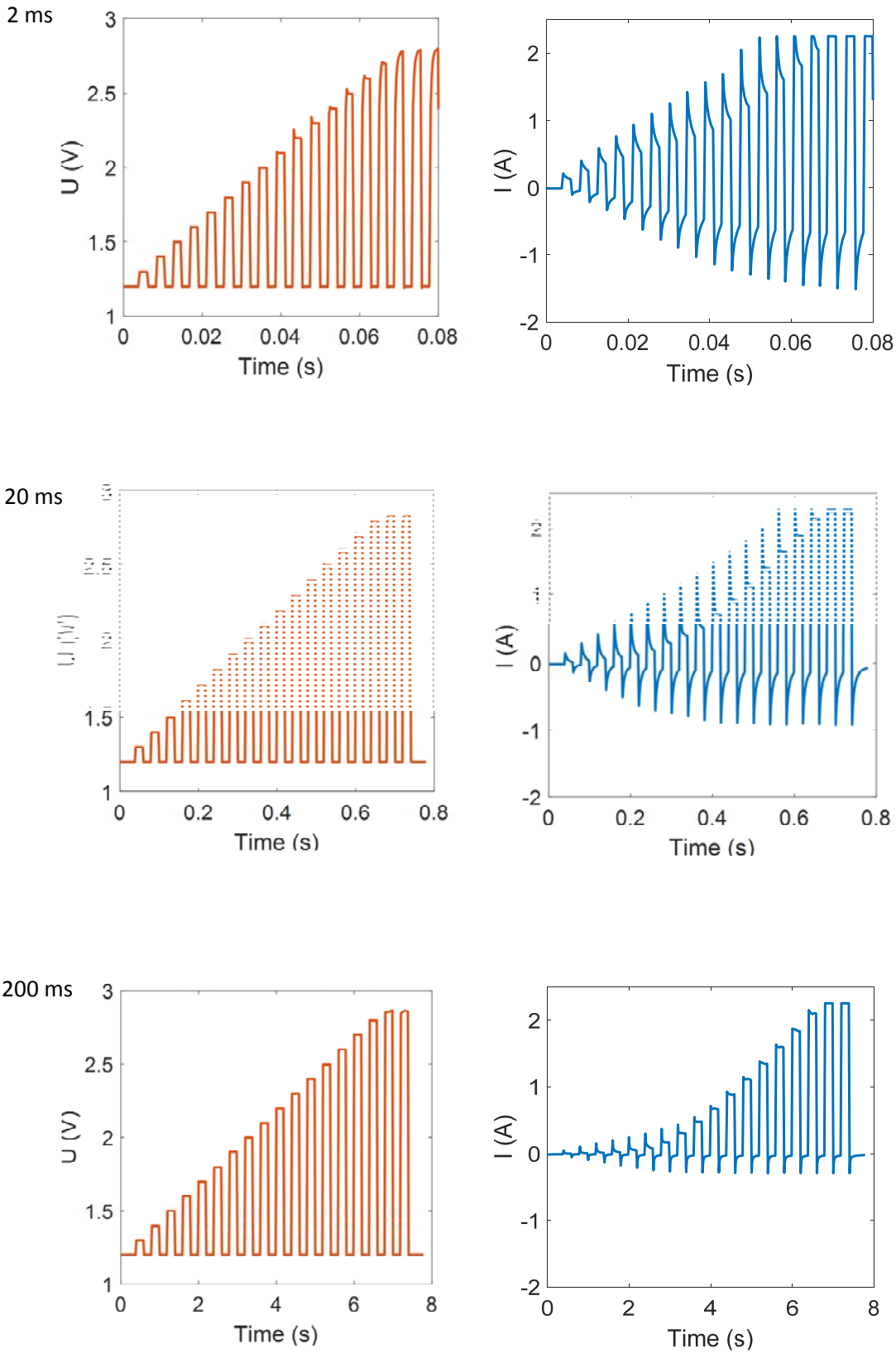

Figure 6

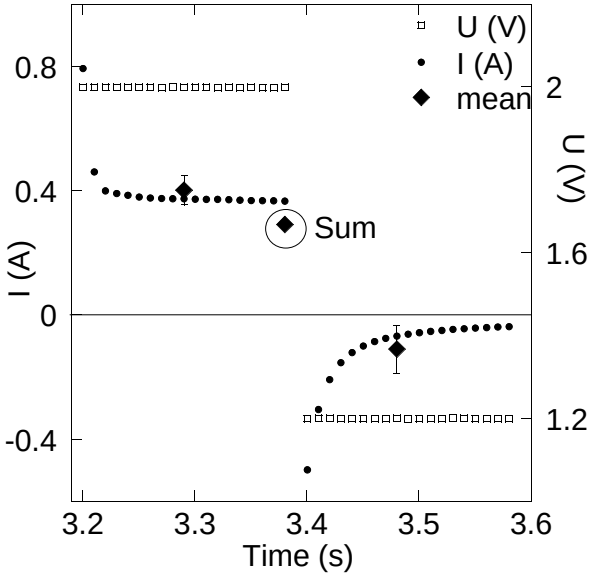

Figure 7

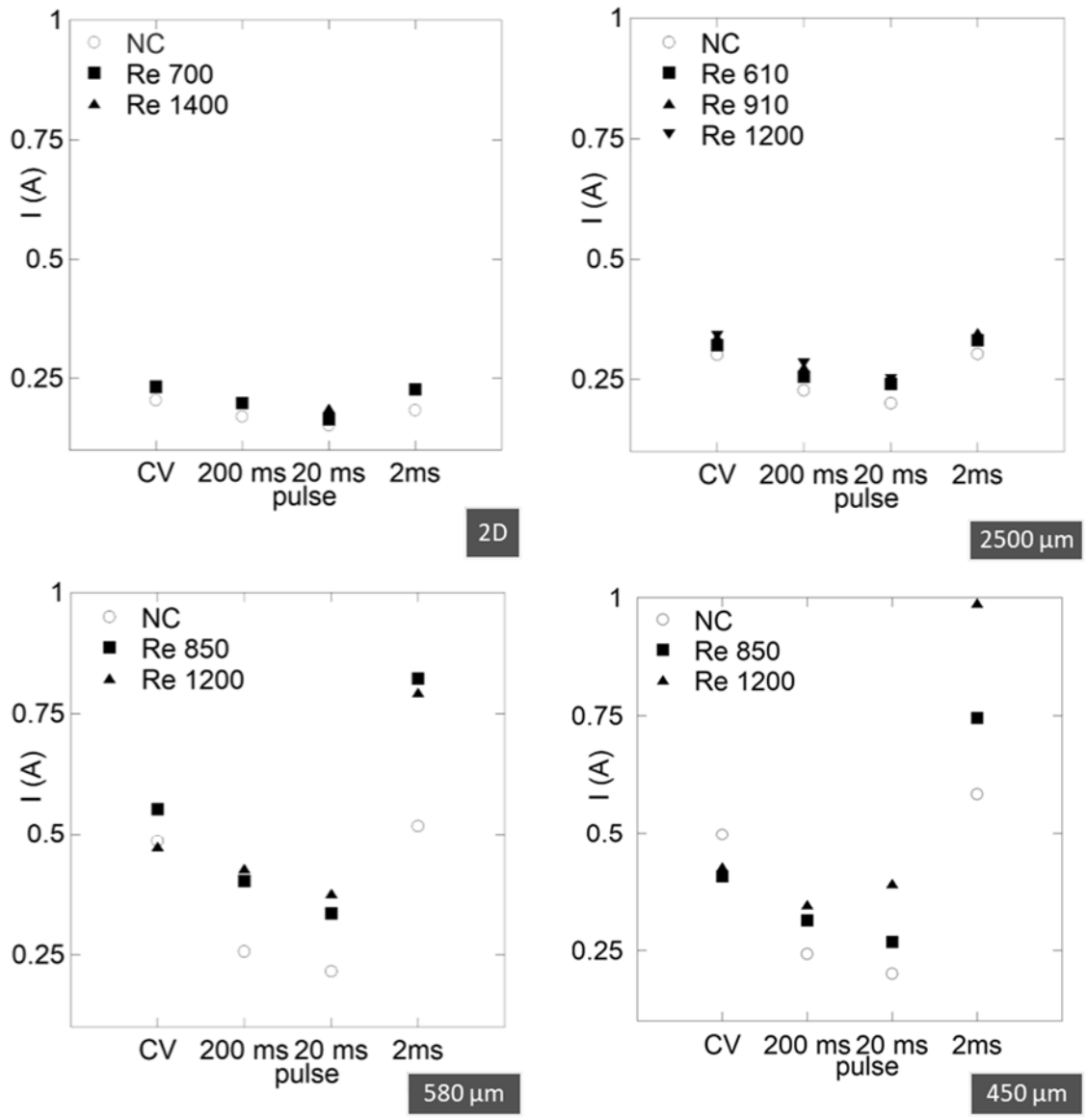
NC
Re 700
Re 1400
I (A)
1
0.75
0.5
0.25
CV
200 ms pulse
20 ms
2ms
2D
NC
Re 610
Re 910
Re 1200
2500 µm
NC
Re 850
Re 1200
580 µm
NC
Re 850
Re 1200
450 µm

Figure 8